HHS Public Access

Author manuscript

Neuroimage. Author manuscript; available in PMC 2017 January 15.

Published in final edited form as:

Neuroimage. 2016 January 15; 125: 848–856. doi:10.1016/j.neuroimage.2015.10.083.

Brain region and activity-dependent properties of M for calibrated fMRI

Christina Y. Shu[1], **Peter Herman**[2], **Daniel Coman**[2], **Basavaraju G. Sanganahalli**[2], **Helen Wang**[2], **Christoph Juchem**[2,3], **Douglas L. Rothman**[1,2], **Robin A. de Graaf**[1,2], and **Fahmeed Hyder**[1,2]

[1]Department of Biomedical Engineering, Yale University, New Haven, CT, USA

[2]Department of Radiology and Biomedical Imaging and Magnetic Resonance Research Center, Yale University, New Haven, CT, USA

[3]Department of Neurology, Yale University, New Haven, CT, USA

Abstract

Calibrated fMRI extracts changes in oxidative energy demanded by neural activity based on hemodynamic and metabolic dependencies of the blood oxygenation level-dependent (BOLD) response. This procedure requires the parameter M, which is determined from the dynamic range of the BOLD signal between deoxyhemoglobin (paramagnetic) and oxyhemoglobin (diamagnetic). Since it is unclear if the range of M-values in human calibrated fMRI is due to regional/state differences, we conducted a 9.4T study to measure M-values across brain regions in deep (α-chloralose) and light (medetomidine) anesthetized rats, as verified by electrophysiology. Because BOLD signal is captured differentially by gradient-echo (R_2*) and spin-echo (R_2) relaxation rates, we measured M-values by the [R2.3] product of the fMRI echo time and R_2' (i.e., the reversible magnetic susceptibility component), which is given by the absolute difference between R_2* and R_2. While R_2' mapping was shown to be dependent on the k-space sampling method used, at nominal spatial resolutions achieved at high magnetic field of 9.4T the M-values were quite homogenous across cortical gray matter. However cortical M-values varied in relation to neural activity between brain states. The findings from this study could improve precision of future calibrated fMRI studies by focusing on the global uniformity of M-values in gray matter across different resting activity levels [R2.1b].

Address correspondence and reprint requests to: Christina Y. Shu / D. S. Fahmeed Hyder, N143 TAC (MRRC), 300 Cedar Street, Yale University, New Haven, CT 06520, U.S.A. Tel: +1-203-785-6205, Fax: +1-203-785-6643, christina.shu@yale.edu / fahmeed.hyder@yale.edu.

Author Contributions: CYS and FH designed study; CYS, PH, BGS conducted study; CYS, PH, DC, HW, FH conducted data analysis; CYS, PH, DC, BGS, HW, CJ, DLR, RAG, FH wrote the paper.

Disclosure/Conflict of Interest: The authors declare that there are no conflicts of interest.

Keywords

blood flow; blood volume; glutamate; lactate; neurometabolic coupling; neurovascular coupling

1. Introduction

In conventional fMRI studies regions of interest are exposed from the stimulus-evoked changes in blood oxygenation level-dependent (BOLD) signal, using deoxyhemoglobin as the endogenous intravascular MRI contrast agent. Given the complex nature of the BOLD contrast, interest in quantitative fMRI has renewed awareness in oxidative energy demanded by the underlying neural activity. Relationships between BOLD signal and neurophysiological parameters allow the determination of changes in cerebral metabolic rate of oxygen consumption (CMR_{O2}) from a baseline condition by calibrated fMRI, requiring multi-modal measurements of BOLD signal along with cerebral blood flow (CBF) and volume (CBV).

CBV is often not measured in human studies (Hoge, 2012), but it can be directly measured in animal studies (Hyder and Rothman, 2012). An important component of calibrated fMRI is the BOLD signal weighting at two extremes: “low” BOLD signal with deoxyhemoglobin (paramagnetic) and “high” BOLD signal with oxyhemoglobin (diamagnetic). The dynamic range of the BOLD signal between these two extremes is reflected by a parameter M, which is believed to be a magnetic field-dependent constant that is tissue-specific (e.g., oxyhemoglobin vs. deoxyhemoglobin ratio, which depends on the resting values of CBV, CBF, and CMR_{O2}) (Hoge, 2012; Hyder and Rothman, 2012).

Since magnetic properties of changing blood oxygenation (Y) affect the tissue water MRI signal through intravoxel spin dephasing (Kennan et al., 1994), the change in Y can be differentially captured with the transverse relaxation rates as measured by gradient-echo (R_2*) and spin-echo (R_2). If the relaxation components in R_2* and R_2 assigned to nonsusceptibility-based effects are ignored (Kida et al., 2000), then under well-shimmed conditions

$$R_2^* \cong R_2'(Y) + R_2(Y) \quad (1a)$$

$$R_2 \cong R_2(Y) \quad (1b)$$

where $R_2'(Y)$ and $R_2(Y)$ represent the blood oxygenation-dependent relaxation components that are reversible (e.g., static magnetic fields inhomogeneity, slow diffusion regime) and irreversible (i.e., intermediate to fast diffusion regime), respectively (Kida et al., 2000). Because at high magnetic field the intravascular weighting of these measured rates is significantly reduced (Kennan et al., 1994; Kida et al., 2000; Silvennoinen et al., 2003), the difference between the two rates (i.e., $R_2' = R_2^* - R_2$) are thought to represent primarily the extravascular susceptibility-induced effects of tissue water (Hyder et al., 2001; Silvennoinen et al., 2003). Then the calibrated fMRI parameter M is simply given by the product between R_2' and the echo time (TE) used in the experiment (Hoge et al., 1999a; Kida et al., 2000).

$$M = TE \cdot R_2' \quad (2)$$

Alternatively, in human calibrated fMRI studies, M is also derived by data fitting using BOLD and CBF data from measurements during gas challenges (CO_2, O_2, or mixtures of the two) (Chiarelli et al., 2007; Davis et al., 1998; Gauthier et al., 2011). However this method requires additional experimental setups (i.e., gas lines, blood gas or exhaled air measurements) and physiological assumptions (i.e., changes in neural activity and/or CMR_{O2} are negligible during gas challenges) (Hoge et al., 1999a).

As recently summarized (Hyder et al., 2013b), a very wide range of M-values have been reported in human calibrated fMRI experiments (Supplementary Figure 1) (Chiarelli et al., 2007; Davis et al., 1998; Gauthier et al., 2011; Hoge et al., 1999b; Kastrup et al., 1999; Stefanovic et al., 2006). Since it remains uncertain if the range of M-values reported in human calibrated fMRI studies are due to regional and/or state differences, this study was designed to test if M can be reliably estimated from direct R_2' measurements under well-shimmed conditions and to examine regional and brain-state dependencies of M-values in the rat brain.

While human calibrated fMRI studies are conducted in the awake state, in rats we can study distinct activity levels by administering different anesthetic agents. Regardless of species, a linear relationship exists between neuronal firing and metabolism across different activity levels (see (Hyder et al., 2013a) and references within). While human brain has lower neuronal firing and metabolic rates compared to rat brain, in both species neuronal firing and metabolic rates increase/decrease with sensory stimuli/anesthesia (vs. the awake state). In humans it is known that neuronal firing and metabolic rates decrease with disease (vs. the awake state). Thus by interpreting M-values in relation to neuronal firing rate measured at varying brain states, we can infer the M-values to altered brain state regardless of species [R2.1] [R2.1a].

2. Materials and Methods

2.1 Animal preparation

All procedures were performed in accordance with protocols approved by the Yale Institutional Animal Care and Use Committee (IACUC) and in agreement with the National Institute of Health *Guide for the Care and Use of Laboratory Animals*. Sprague-Dawley rats (male, ~300 g) were artificially ventilated (70% N_2O, 30% O_2) to maintain normal physiology and anesthetized with α-chloralose (i.p. 80 mg/kg initial dose, then 40mg/kg/hr, n = 8) or medetomidine hydrochloride (i.v. 0.1mg/kg/hr, n = 7). A femoral arterial line was used for monitoring blood pressure (90±10 mmHg), pH (7.4±0.2), and blood gases (pO_2 = 100±15 mmHg, pCO_2 = 37±3 mmHg).

2.2 Electrophysiology experiments

Six anesthetized rats (n = 3 each with α-chloralose and medetomidine) were mounted on a stereotaxic holder sitting on a vibration-free table inside a Faraday cage. Tiny burr holes above the forepaw (i.e., $S1_{FL}$) somatosensory regions (4.4 mm lateral and 1.0 mm anterior to

Bregma) were drilled and high-impedance tungsten microelectrodes (FHC Inc) were inserted. Recording of neural signals was performed with a micro 1401 A/D converter unit using Spike2 software (CED). Multiunit activity (MUA) and local field potential (LFP) were isolated from the raw signal with band pass (0.3-3 kHz) and low pass (<150 Hz) electronic filters (Krohn-Hite Inc), respectively.

2.3 Image acquisition

The MRI data were obtained on a 9.4T system interfaced to a Direct Drive console (Agilent Tech, Santa Clara, CA) and an actively shielded gradient coil with 500 mT/m maximum gradient strength at 180 μs rise time (Magnex, UK). We used a custom-built ^{1}H dual quadrature surface coil (each coil's diameter was 3.5 cm) and the static magnetic field inhomogeneity was optimized with second-order spherical harmonics shimming until the half-height line width of water across nearly the entire brain was 15-20 Hz (Supplementary Figure 2) (Juchem et al., 2014). Both conventional spin-wrap two-dimensional-Fourier-Transform (2DFT) and echo-planar-imaging (EPI) sequences were used in the gradient-echo (GE) and spin-echo (SE) experiments. The parameters used for 2DFT (GE/SE) were: recycle time (TR) = 500 ms/3000 ms, echo time (TE) = 5-40 ms/10-100 ms, number of echoes (NE) = 8/10 [R1.1], number of averages (NA) = 4/1, number of dummy scans (ND) = 16/8, excitation pulse = 45° sinc/90° sinc, and field-of-view (FOV) = 32×32 mm with scan durations = approximately 7/4 minutes. The parameters used for EPI (GE/SE) were: TR = 1000 ms/2000 ms, TE = 15-45 ms/32-92 ms, NE = 7/7 [R1.1], NA = 4/1, ND = 16/8, excitation pulse = 90° sinc/90° sinc, and FOV = 32×32 mm. EPI images were acquired at different TE separately, with a scan time of approximately 5 minutes for GE and 3 minutes for SE. For 2DFT and EPI acquisitions, the slice thickness (0.3-1 mm) and in-plane resolution (64×64, 128×128, 256×256) were varied as required by our experimental goals.

2.4 Data processing

Data were processed off-line in MATLAB (MathWorks, Natick, MA, USA) and the Bioimage Suite program package (www.bioimagesuite.org) (Papademetris et al., 2006). R_2 and R_2* images from 2DFT were calculated based on exponential decay fittings of GE and SE signal intensities vs. TE values. To examine whether residual contributions from spin-echo components were completely refocused in 2DFT acquisitions, both single- and multi-exponential decay models were used to fit for R_2 [R1.2]. R_2' images were calculated as the absolute difference between R_2* and R_2, and M was calculated by eq. (2) with a TE of 15 ms. All images were registered to a reference atlas (scalablebrainatlas.incf.org), after which cerebral spinal fluid (CSF) was masked out and edge artifacts due to misregistration were removed. Signal-to-noise ratio (SNR) was calculated as the ratio between average signal intensities of voxels inside and outside the brain.

A template (Calabrese et al., 2013) was overlaid on the images to calculate mean values in 22 regions of interest (ROIs). Only ROIs minimally affected by residual shimming artifacts were chosen for analysis (Supplementary Figure 2) (Juchem et al., 2014).

The selected ROIs included: Internal capsule (ic), Septum (Spt), Diagonal domain (DiagD), Striatum (Str), Diencephalon (Dien), Hippocampal formation (Hif), Pallidum (GP),

Accumbens (Acb), Fimbria fornix (fi), Preoptic area (POA), Bed nuclei stria terminalis (BNST), Corpus callosum (cc), Olfactory structure (Olf), Visual cortex: primary (V1), Visual cortex: secondary (V2), Motor cortex: primary (M1), Motor cortex: secondary (M2), Primary somatosensory cortex: fore-limb ($S1_{FL}$), Primary somatosensory cortex: upper-lip ($S1_{ULP}$), Primary somatosensory cortex: hind-limb ($S1_{HL}$), Somatosensory cortex: barrel fields ($S1_{BF}$), Secondary somatosensory cortex (S2).

To gain insight for the overall regional behavior of R_2, R_2*, and R_2', these ROIs were categorized into “white matter”, “cortical gray matter”, or “subcortical gray matter”. Diencephalon covered both gray and white matter and therefore was not included in any group. Two-way analysis of variance (ANOVA) and Student's t-test were used to compare regional R_2' values under α-chloralose and medetomidine.

3. Results

Physiological parameters such as blood pH, pCO_2, and pO_2 for all rats in each group were maintained within normal limits throughout the scans (Table 1). All results are shown as mean ± standard deviation (SD).

3.1 Neural activity under α-chloralose vs. medetomidine

The MUA and LFP recordings from $S1_{FL}$ revealed significant differences in neural activity between α-chloralose and medetomidine (Figure 1). The LFP in α-chloralose group had a root mean square (RMS) of 1.3±0.1 and a spike rate of 4.2±1.1Hz, whereas the medetomidine group had an LFP_{RMS} of 3.0±0.7 and a spike rate of 7.3±1.1Hz. In other words, medetomidine rats showed roughly a doubling of neural activity vs. α-chloralose rats ($p < 0.05$).

3.2 Comparison of R_2, R_2*, and R_2' across regions

We obtained R_2, R_2*, R_2', and M maps for rats under α-chloralose and calculated mean±SD for each ROI (Figure 2A). For 2DFT acquisitions, R_2 values fitted with single- and multi-exponential decays were identical, and thus only data in the former case are reported [R1.2]. There were no observed patterns of similarity between regional variations of the ROI volumes (Figure 2B) and R_2' (Figure 2C) suggesting that, with good field homogeneity, our analysis was not biased by the size of ROI. Across all ROIs, R_2 ranged from 16.1 to 24.1 s^{-1}, R_2* ranged from 31.4 to 44.5 s^{-1}, and R_2' ranged from 10.6 to 20.9 s^{-1}. In gray matter ROIs, R_2, R_2*, and R_2' were generally more homogeneous in the cortical areas compared to subcortical areas. Two-way ANOVA on the neocortical gray matter ROIs suggested that they were not significantly different from each other ($p > 0.05$). Among all ROIs, a minimum R_2' value was found in M1 (10.6±1.1 s^{-1}) while the maximum was found in ic (20.9±3.5 s^{-1}). There was a strong linear correlation between R_2' and R_2* ($r^2 = 0.86$).

3.3 Sensitivity of R_2, R_2*, and R_2' to imaging resolution and imaging sequence

From the default imaging resolution of 128×128 k-space matrix size with 0.5 mm slice thickness, we varied resolutions (Figure 3) for through-plane (i.e., by varying slice thickness) and in-plane (i.e., by varying image matrix), and used different k-space sampling

methods (Figure 4) for imaging (i.e., 2DFT and EPI). These data were collected from the same α-chloralose rats.

Figure 3 shows that R_2 and R_2* with different in-plane resolutions did not produce significantly different R_2' values ($p > 0.05$). At the whole brain level, at default setting (128×128 in-plane, 0.5 mm slice), R_2' was 14.1±9.5 s^{-1}. Changing the matrix size to 64×64 and 256×256 produced R_2' values of 15.4±11.0 and 13.9±9.2 s^{-1}. R_2' values remained similar with 1 mm and 0.3 mm slices ($p > 0.05$ for 0.3mm). From the default setting, changing slice thickness to 1 mm and 0.3 mm produced R_2' values of 17.4±12.8 and 13.4±9.5 s^{-1}, respectively (Table 2).

In Figure 4, R_2 values in EPI appear more heterogeneous than R_2 values in 2DFT. Additionally, higher R values were generally reported with EPI. In gradient-echo experiments, stronger magnetic susceptibility near large vessels undermined R_2* fitting because of significant signal drop out areas; this in turn led to R_2* heterogeneity near these voxels. Due to these heterogeneities in R_2 and R_2* the R_2' and M maps with EPI were less uniform compared to the R_2' and M maps with 2DFT (Figure 4A). Figures 4B-D compares the distributions of R_2, R_2*, and R_2' values measured by 2DFT (dotted line) and EPI (solid line) for a series of voxels located horizontally across the coronal slice whose location corresponded to the magenta line on the anatomical image shown in Figure 4A. The intensity profiles of EPI exhibited more variations in the R_2, R_2*, R_2' and M maps compared to the intensity profiles of 2DFT maps.

3.4 Comparison of M across brain states

M-values with α-chloralose (M_α) vs. medetomidine (M_{med}) are shown in Figure 5. Taking all ROIs into account, M-values between two states were well correlated ($r^2 = 0.85$), although the correlations were similar in white matter and cortical gray matter ($r^2 = 0.89$ and 0.75). General features across all ROIs were nearly identical between M_α and M_{med}. In the whole brain, for both states, M had a maximum in ic. In the subcortex, for both states, M had a maximum in DiagD and a minimum in Spt.

Among all ROIs, M_α was 22.2±8.5 and M_{med} was 19.6±8.2, which corresponded to about a 12% drop in M-values from α-chloralose to medetomidine. In the subcortical gray matter, M_α was 21.7±9.0 and M_{med} was 18.7±7.9. In the cortical gray matter, M_α was 17.3±4.8 and M_{med} was 14.7±4.7. In all of white matter, M_α was 23.6±7.8 and M_{med} was 22.5±8.0. Two-way ANOVA test showed that M_{med} were significantly lower than M_α for both cortical ($p < 0.0001$) and subcortical regions ($p < 0.05$) but not in white matter and diencephalon ($p > 0.05$). In both cortical and subcortical gray matter, there was an average of 15% difference in M-values between α-chloralose and medetomidine.

4. Discussion

In calibrated fMRI, the parameter M is given by the product of R_2' and TE, and it depends on multiple physiological and experimental parameters (Hoge et al., 1999a). At high magnetic fields (>4T) the extravascular R_2' component dominates, but at lower fields (<4T) the BOLD signal contains a significant intravascular component (Donahue et al., 2011;

Silvennoinen et al., 2003). Since the calibrated fMRI model assumes that the intravascular component is eliminated (or non-contributing), comparison of M-values across different magnetic fields (Supplementary Figure 1) should account for the intravascular contributions. Calibrated fMRI at 9.4T, as done here, is intrinsically weighted to the extravascular R_2' component and the high-spatial resolution renders minimal partial volume artifacts across gray and white matter.

4.1 M-values with respect to image resolution and imaging sequence

To test the robustness of the R_2' mapping method, we varied image resolution both in-plane and through-plane (Figure 3; Table 2). While the SNR in gradient-echo and spin-echo images at each TE drop with higher resolution (Supplementary Figure 3), the corresponding R_2' values did not vary significantly, suggesting that within reasonable imaging resolution (where SNR is not significantly decreased) M can be quite reliably measured with this method. Since R_2' values were fairly similar when decreasing the voxel size from 128×128 to 256×256 image matrix with 0.5 mm slices and from 0.5 mm slice to 0.3 mm slice at 128×128 image matrix, we believe this range of imaging resolutions to be optimally suited for R_2' mapping in rat brain.

While keeping the spatial resolution constant, k-space sampling method was varied between EPI and 2DFT (Figure 4). Most R_2 values with EPI were higher than values measured with 2DFT. The identical R_2 values with 2DFT between single- and multi-exponential fittings confirmed complete refocusing at 9.4T [R1.2]. However, because the spin-echo sequence in EPI uses asymmetric spin-echoes, even under good shimming conditions the R_2 component measured by EPI may have some residual contributions from components that are not completely refocused (Stables et al., 1998). This is known to contribute to multi-exponential behavior (Blockley et al., 2015; Yablonskiy and Haacke, 1997) and needs to be minimized by post-acquisition methods. Compared to the R_2* measured by 2DFT, the R_2* component measured by EPI is more sensitive to static field inhomogeneity terms near poorly shimmed regions because of the high bandwidth requirements for the faster k-space sampling needed for EPI. Both R_2 and R_2* maps acquired with EPI showed greater heterogeneity compared to 2DFT, which led to larger voxel-to-voxel variations in the R_2' maps obtained by EPI (vs. 2DFT). The differences in R_2' maps derived with EPI and 2DFT in our study may explain, in part, the heterogeneity of M-values reported in the existing calibrated fMRI literature for human brain (Supplementary Figure 1).

4.2 M-values across different brain regions and activity states

In general, the human calibrated fMRI literature at 3T shows widespread M-values both within the same cortical region (e.g., visual cortex) and across different cortical regions (e.g., visual and motor cortices) (Supplementary Figure 1). The maximum M-value (14.7) was more than triple the minimum M-value (4.3) with a mean M-value of 9.1±4.3. In our study of α-chloralose and medetomidine rats (Figure 5), we observed a much smaller range of regional differences across all ROIs in the brain, but higher M-values. In α-chloralose rats the maximum M-value (31.3) was less than double the minimum M-value (15.9), with a mean M-value of 21.0±4.0. Between the primary visual and motor cortices, average M-values were between ∼16 and ∼17. Similarly, at 3T Blockley et al measured M-values by

two different methods in human cerebral cortex: hypercapnia challenge and R_2' method. They found small difference in M-values between visual cortex and the whole gray matter with the R_2' method, but regional variations in M-values increased significantly with the hypercapnia challenge (Blockley et al., 2015). Their study, in agreement with our observations, suggests that regional M variations may, in part, be dependent on the method used (i.e., hypercapnia vs. R_2' mapping), where R_2' mapping shows less variations in M-values across regions.

The higher M-values observed in white matter relative to gray matter could be partly attributed to the susceptibility of myelin, as a previous study found that at 9.4T R_2' measured in the white matter of normal mouse was higher by 10 s^{-1} than R_2' measured in demyelinated white matter of mouse on a cuprizone diet (Lee et al., 2012) [R1.3] [R3.1]. We found that with different brain activity levels M (or R_2') does not change in white matter, but M (or R_2') changes in gray matter. Since the lack of change in white matter with activity could also be due to alterations in myelin susceptibility and iron content cancelling out changes due to vascular factors, future studies will be needed to further assess this possibility. Given that calibrated fMRI is mainly focused towards gray matter changes, the white matter should be masked for quantification of CMR_{O2} changes from calibrated fMRI data [R1.4].

Most human calibrated fMRI studies are conducted in the awake state, but with animal models different anesthesia can be applied to achieve different levels of global brain activity. These different states - which have been characterized by magnetic resonance spectroscopy (MRS), positron emission tomography (PET), and electrophysiology - possess distinct levels of metabolic and electrical activity (Hyder et al., 2013a). The R_2' method for calibrated fMRI has been validated by both CMR_{O2} and neural activity measurements. Kida et al calculated CMR_{O2} changes in rat brain by calibrated fMRI using R_2' mapping at 7T in conjunction with CBF and CBV mapping. The calculated CMR_{O2} changes were validated by proton-observed carbon-edited (POCE) MRS, where from a control state Kida et al reported higher CMR_{O2} with light anesthesia and lower CMR_{O2} with deep anesthesia (Kida et al., 2000). Similarly, rat studies during sensory stimulation have compared CMR_{O2} changes predicted by calibrated fMRI at 11.7T with changes in neuronal activity measured directly by electrophysiology (Herman et al., 2013; Sanganahalli et al., 2009; Smith et al., 2002).

A very popular anesthetic for rodent functional studies is α-chloralose because it potentiates evoked responses and attenuates cardiovascular or reflex functions (Bonvento et al., 1994; Lindauer et al., 1993; Ueki et al., 1992; Winters, 1976). But α-chloralose, which affects mainly via the $GABA_A$ receptors (Garrett and Gan, 1998), is used only in terminal experiments. Medetomidine is an injectable α2-adrenergic agonist with a short half-life and more suitable for longitudinal studies (Weber et al., 2006). α2-agonists stimulates adrenergic α2 receptors located pre-synaptically in the central nervous system, resulting in inhibition of the release of norepinephrine, and several other mediators from the nerve terminals (Scheinin and MacDonald, 1989). Medetomidine, therefore, causes analgesia (Langer et al., 1985) to create a sleep-like sedated state (Huupponen et al., 2008; Nelson et al., 2003). Several fMRI studies demonstrated the use of medetomidine for both resting-state

and task-based paradigms (Pawela et al., 2009; Weber et al., 2006; Zhao et al., 2008). These studies suggest that the BOLD impulse response function, derived from spontaneous or evoked neural activity, vary between α-chloralose and medetomidine anesthesia and imply that the neurovascular coupling between these two states are different (Herman et al., 2011). To quantify the difference in neural activity between the two brain states induced by these different anesthesia mechanisms, we conducted MUA and LFP recordings in anesthetized rats. The medetomidine group exhibited neural activity approximately twice as high as detected with α-chloralose (Figure 1).

In terms of magnitude of M between α-chloralose and medetomidine, a two-way ANOVA test suggested M-values in medetomidine was significantly lower than M-values in α-chloralose in both cortical and subcortical gray matter, but not in white matter and diencephalon (Figure 5). Despite the change in M-value being significant from α-chloralose to medetomidine, the relative difference was small (∼12%) compared to the relative difference observed in neural activity (∼100%). In a previous study, Kida et al. compared M-values measured between rats sedated with morphine (light sedation level) and pentobarbital (deep sedation level) (Kida et al., 2000). Similar to our observations, the morphine-induced state represented roughly a 250% higher glucose metabolic rate compared to the pentobarbital-induced state, whereas the relative decrease in M-value was only about 26% (Kida et al., 2000). Given the linear relationship between neuronal activity and metabolic rates in mammalian brain (Hyder et al., 2013a), the change in M-value (about 10-25%) in relation to neuronal activity or metabolic rates (about 100-250%) observed in the present study and the Kida et al. study are in good agreement [R2.1]. Moreover both in the Kida et al. study and this present study, M (or R_2') is decreased (i.e. BOLD signal increased) when the brain activity/metabolism is increased. In the future, characterizing dependencies of M-values over a range of neural activities will give insights as to how the dynamic range of the BOLD signal is related to baseline neuronal activity or metabolic rates.

The regional pattern of M-value was conserved across brain states (Figure 5). All extremes in M-values were in very similar regions (ic, Olf, DiagD, and Spt) in both brain states. Particularly, in both states the neocortical M-values were invariant among themselves and the regional differences were not as large as variations in cortical M-values observed in the human calibrated fMRI literature (Supplementary Figure 1). Thus regardless of the brain state, M-values across different regions in the cerebral cortex were very similar. Since M is a function of CBV, CBF, and CMR_{O2}, the near constancy of M-values across neocortical ROIs implies similar level of flow-metabolism coupling in most of cortical gray matter (Hoge et al., 1999a; Hyder et al., 2000), for both α-chloralose and medetomidine. It should be noted, however, that we expect absolute differences of CBF and CMR_{O2} between α-chloralose and medetomidine states.

4.3 M-values measured by other methods at different magnetic field strengths

While calibrated fMRI is based on a model of the extravascular BOLD signal, it has been suggested that at magnetic fields lower than 7T the BOLD signal contains significant intravascular contributions, e.g., nearly one third of the total BOLD response (Donahue et al., 2011; Silvennoinen et al., 2003). While the R_2' method used in this study at 9.4T would

effectively eliminate the intravascular water signal allowing accurate values of M to be determined, it may be further necessary that the intravascular signal be further suppressed (e.g., by using in-flow spoiler gradients) or be removed on the basis of post-processing [R2.2].

It is difficult to assess if M-values vary with magnetic field strength from existing calibrated fMRI studies in humans (Supplementary Figure 1). Based on the limited number of studies utilizing the R_2' mapping method, previous and present R_2' measurements do not seem to suggest that M-values vary significantly with magnetic field strength.

M is a function of TE used in the fMRI study, and shorter TE applied at higher field strengths should be taken into consideration when comparing R_2'-derived M-values with respect to field strength. For example, Sedlacik et al measured R_2' at 3T in human brain and reported R_2' values of 9.8 s^{-1} in the occipital cortex, which translates to an M-value of ∼20 with a TE of 20 ms (Sedlacik et al., 2014). But as discussed above, for studies at 4T and lower the R_2' should be separated into intravascular and extravascular components. Considering only the extravascular component at 3T for Sedlacik et al, the M-value should be adjusted to about 14. Similarly Blockley et al determined M to be ∼11 and ∼9 in the visual cortex and all of gray matter, respectively, at 3T (Blockley et al., 2015). In our study at 9.4T we found M-values in visual and somatosensory cortices were in the range of 15-17 across the different brain states, and in the awake state M might be slightly lower than 15 (since M decreases slightly at higher activity levels (Kida et al., 2000)). Kida et al showed that R_2' in somatosensory cortex at 7T was 8.2 s^{-1} for deeply sedated level of anesthesia, which for a TE of 17 ms gave an M-value of about 14 (Kida et al., 2000). The marginal difference of M-values measured at different field strengths (e.g., for $S1_{FL}$ ∼14 at 7T by Kida et al and ∼16 at 9.4T in the present study) suggests that the dynamic range for the extravascular component of the BOLD signal may be quite similar across magnetic fields. However similar studies, as shown here, are needed to confirm this proposition. But it should be noted that the k-space sampling method used for imaging may also impact the derived M-value (see above).

In human calibrated fMRI studies M is determined mainly by data fitting of BOLD vs. CBF changes as the subject breathes CO_2-rich and/or O_2 gas (Chiarelli et al., 2007; Gauthier and Hoge, 2013; Hoge et al., 1999a; Mark et al., 2011). This approach involves an experimental setup for gas exposure and specific assumptions (e.g., constant neural activity and/or CMR_{O2} when gas is introduced). To derive M, it should be noted that the experimental data obtained for BOLD and CBF changes during the gas exposures represent a very small pseudo-linear portion of a highly non-linear (i.e., asymptotic) relationship between large CBF changes in relation to smaller BOLD signal changes (Supplementary Figure 4). The measured CBF increases during gas exposure are less than 100% (Davis et al., 1998; Gauthier et al., 2012), whereas the exponential fitting that defines the M-value from the asymptotic limit revealing the dynamic range of the BOLD signal is reached when CBF increases by several times higher (Gauthier and Hoge, 2013; Hoge et al., 1999a). Moreover, it is difficult to reach large CBF changes in humans without inducing adverse cognitive effects and changes in neural or metabolic activities (Rodgers et al., 2013; Sicard and Duong, 2005; Thesen et al., 2012; Xu et al., 2011; Zappe et al., 2008). Because the data

fitting to derive M-value is susceptible to inaccuracies of both BOLD and CBF measurements, small experimental errors in BOLD or CBF measurements can substantially deviate the M-value derived from the asymptotic fitting (Supplementary Figure 4).

The precision of the asymptotic fitting for M-value can be improved by utilizing the results from this study. We demonstrated that regardless of brain activity levels M-value is largely uniform within neocortex and furthermore its magnitude in corpus callosum is state-independent. Thus future gas exposure methods used in calibrated fMRI studies could consider measuring the M-value in at multiple regions in the cerebral cortex while also measuring the M-value in the corpus callosum. When these measurements are made for at least two brain states (e.g., hypercapnia vs. hyperoxia), the fitting results across regions could be set to match the trends of M-values demonstrated in this study. Moreover, if the metabolic state is in fact unaltered by hypercapnia (Chen and Pike, 2010; Hoge, 2012), then the M-values under α-chloralose and medetomidine, as measured by gas challenge technique, should be comparable to the results shown in Figure 4 [R2.1]. Furthermore human studies could also benefit from the direct R_2' mapping method because magnetic field inhomogeneities are less pronounced at lower magnetic fields and hence the potential artifacts in the M measurements could be significantly reduced as needed for precise calibrated fMRI measurements.

5. Summary

The direct R_2' mapping at nominal spatial resolutions reported M-values that were homogenous across cortical gray matter. But the k-space sampling method for R_2' mapping may influence the reported M-values. While the pattern of regional variations in M-values throughout the brain was nearly identical in both brain states, M-values in cortex varied in relation to neural activity between states. However the direct R2′ mapping method showed cortical uniformity of M-values and which should improve precision of calibrated fMRI further.

Supplementary Material

Refer to Web version on PubMed Central for supplementary material.

Acknowledgments

Thanks to Xenophon Papademetris for inputs on image analysis software and Bei Wang for assistance in animal surgeries. Supported by NIH grants (R01 MH-067528, R01 AG-034953, P30 NS-052519).

References

Blockley NP, Griffeth VE, Simon AB, Dubowitz DJ, Buxton RB. Calibrating the BOLD response without administering gases: Comparison of hypercapnia calibration with calibration using an asymmetric spin echo. Neuroimage. 2015; 104:423–429. [PubMed: 25451475]

Bonvento G, Charbonne R, Correze JL, Borredon J, Seylaz J, Lacombe P. Is alpha-chloralose plus halothane induction a suitable anesthetic regimen for cerebrovascular research? Brain Res. 1994; 665:213–221. [PubMed: 7895056]

Calabrese E, Badea A, Watson C, Johnson GA. A quantitative magnetic resonance histology atlas of postnatal rat brain development with regional estimates of growth and variability. Neuroimage. 2013; 71:196–206. [PubMed: 23353030]

Chen JJ, Pike GB. Global cerebral oxidative metabolism during hypercapnia and hypocapnia in humans: implications for BOLD fMRI. J Cereb Blood Flow Metab. 2010; 30:1094–1099. [PubMed: 20372169]

Chiarelli PA, Bulte DP, Wise R, Gallichan D, Jezzard P. A calibration method for quantitative BOLD fMRI based on hyperoxia. Neuroimage. 2007; 37:808–820. [PubMed: 17632016]

Davis TL, Kwong KK, Weisskoff RM, Rosen BR. Calibrated functional MRI: mapping the dynamics of oxidative metabolism. Proc Natl Acad Sci U S A. 1998; 95:1834–1839. [PubMed: 9465103]

Donahue MJ, Hoogduin H, van Zijl PC, Jezzard P, Luijten PR, Hendrikse J. Blood oxygenation level-dependent (BOLD) total and extravascular signal changes and DeltaR2* in human visual cortex at 1.5, 3.0 and 7.0 T. NMR Biomed. 2011; 24:25–34. [PubMed: 21259367]

Garrett KM, Gan J. Enhancement of gamma-aminobutyric acidA receptor activity by alpha-chloralose. J Pharmacol Exp Ther. 1998; 285:680–686. [PubMed: 9580613]

Gauthier CJ, Desjardins-Crepeau L, Madjar C, Bherer L, Hoge RD. Absolute quantification of resting oxygen metabolism and metabolic reactivity during functional activation using QUO2 MRI. Neuroimage. 2012; 63:1353–1363. [PubMed: 22986357]

Gauthier CJ, Hoge RD. A generalized procedure for calibrated MRI incorporating hyperoxia and hypercapnia. Hum Brain Mapp. 2013; 34:1053–1069. [PubMed: 23015481]

Gauthier CJ, Madjar C, Tancredi FB, Stefanovic B, Hoge RD. Elimination of visually evoked BOLD responses during carbogen inhalation: implications for calibrated MRI. Neuroimage. 2011; 54:1001–1011. [PubMed: 20887792]

Herman P, Sanganahalli BG, Blumenfeld H, Rothman DL, Hyder F. Quantitative basis for neuroimaging of cortical laminae with calibrated functional MRI. Proc Natl Acad Sci U S A. 2013; 110:15115–15120. [PubMed: 23980158]

Herman P, Sanganahalli BG, Hyder F, Eke A. Fractal analysis of spontaneous fluctuations of the BOLD signal in rat brain. Neuroimage. 2011; 58:1060–1069. [PubMed: 21777682]

Hoge RD. Calibrated FMRI. Neuroimage. 2012; 62:930–937. [PubMed: 22369993]

Hoge RD, Atkinson J, Gill B, Crelier GR, Marrett S, Pike GB. Investigation of BOLD signal dependence on cerebral blood flow and oxygen consumption: the deoxyhemoglobin dilution model. Magn Reson Med. 1999a; 42:849–863. [PubMed: 10542343]

Hoge RD, Atkinson J, Gill B, Crelier GR, Marrett S, Pike GB. Linear coupling between cerebral blood flow and oxygen consumption in activated human cortex. Proc Natl Acad Sci U S A. 1999b; 96:9403–9408. [PubMed: 10430955]

Huupponen E, Maksimow A, Lapinlampi P, Sarkela M, Saastamoinen A, Snapir A, Scheinin H, Scheinin M, Merilainen P, Himanen SL, Jaaskelainen S. Electroencephalogram spindle activity during dexmedetomidine sedation and physiological sleep. Acta Anaesthesiol Scand. 2008; 52:289–294. [PubMed: 18005372]

Hyder F, Fulbright RK, Shulman RG, Rothman DL. Glutamatergic function in the resting awake human brain is supported by uniformly high oxidative energy. J Cereb Blood Flow Metab. 2013a; 33:339–347. [PubMed: 23299240]

Hyder F, Kennan RP, Kida I, Mason GF, Behar KL, Rothman D. Dependence of oxygen delivery on blood flow in rat brain: a 7 tesla nuclear magnetic resonance study. J Cereb Blood Flow Metab. 2000; 20:485–498. [PubMed: 10724113]

Hyder F, Kida I, Behar KL, Kennan RP, Maciejewski PK, Rothman DL. Quantitative functional imaging of the brain: towards mapping neuronal activity by BOLD fMRI. NMR Biomed. 2001; 14:413–431. [PubMed: 11746934]

Hyder F, Rothman DL. Quantitative fMRI and oxidative neuroenergetics. Neuroimage. 2012; 62:985–994. [PubMed: 22542993]

Hyder, F.; Shu, CY.; Herman, P.; Sanganahalli, BG.; Coman, D.; Rothman, DL. Quantifying morphology and physiology of the human body using MRI. In: Muftuler, LT., editor. Series in medical physics and biomedical engineering. CRC Press/Taylor & Francis Group; Boca Raton, FL: 2013b. p. 99-124.

Juchem C, Herman P, Sanganahalli BG, Brown PB, McIntyre S, Nixon TW, Green D, Hyder F, de Graaf RA. DYNAmic Multi-coIl TEchnique (DYNAMITE) shimming of the rat brain at 11.7 T. NMR Biomed. 2014; 27:897–906. [PubMed: 24839167]

Kastrup A, Kruger G, Glover GH, Moseley ME. Assessment of cerebral oxidative metabolism with breath holding and fMRI. Magn Reson Med. 1999; 42:608–611. [PubMed: 10467308]

Kennan RP, Zhong J, Gore JC. Intravascular susceptibility contrast mechanisms in tissues. Magn Reson Med. 1994; 31:9–21. [PubMed: 8121277]

Kida I, Kennan RP, Rothman DL, Behar KL, Hyder F. High-resolution CMR(O2) mapping in rat cortex: a multiparametric approach to calibration of BOLD image contrast at 7 Tesla. J Cereb Blood Flow Metab. 2000; 20:847–860. [PubMed: 10826536]

Langer SZ, Duval N, Massingham R. Pharmacologic and therapeutic significance of alpha-adrenoceptor subtypes. J Cardiovasc Pharmacol. 1985; 7(Suppl 8):S1–8. [PubMed: 2417042]

Lee J, Shmueli K, Kang BT, Yao B, Fukunaga M, van Gelderen P, Palumbo S, Bosetti F, Silva AC, Duyn JH. The contribution of myelin to magnetic susceptibility-weighted contrasts in high-field MRI of the brain. Neuroimage. 2012; 59:3967–3975. [PubMed: 22056461]

Lindauer U, Villringer A, Dirnagl U. Characterization of CBF response to somatosensory stimulation: model and influence of anesthetics. Am J Physiol. 1993; 264:H1223–1228. [PubMed: 8476099]

Mark CI, Fisher JA, Pike GB. Improved fMRI calibration: precisely controlled hyperoxic versus hypercapnic stimuli. Neuroimage. 2011; 54:1102–1111. [PubMed: 20828623]

Nelson LE, Lu J, Guo T, Saper CB, Franks NP, Maze M. The alpha2-adrenoceptor agonist dexmedetomidine converges on an endogenous sleep-promoting pathway to exert its sedative effects. Anesthesiology. 2003; 98:428–436. [PubMed: 12552203]

Papademetris X, Jackowski MP, Rajeevan N, DiStasio M, Okuda H, Constable RT, Staib LH. BioImage Suite: An integrated medical image analysis suite: An update. Insight J. 2006; 2006:209. [PubMed: 25364771]

Pawela CP, Biswal BB, Hudetz AG, Schulte ML, Li R, Jones SR, Cho YR, Matloub HS, Hyde JS. A protocol for use of medetomidine anesthesia in rats for extended studies using task-induced BOLD contrast and resting-state functional connectivity. Neuroimage. 2009; 46:1137–1147. [PubMed: 19285560]

Rodgers ZB, Jain V, Englund EK, Langham MC, Wehrli FW. High temporal resolution MRI quantification of global cerebral metabolic rate of oxygen consumption in response to apneic challenge. J Cereb Blood Flow Metab. 2013; 33:1514–1522. [PubMed: 23838827]

Sanganahalli BG, Herman P, Blumenfeld H, Hyder F. Oxidative neuroenergetics in event-related paradigms. J Neurosci. 2009; 29:1707–1718. [PubMed: 19211878]

Scheinin M, MacDonald E. An introduction to the pharmacology of alpha 2-adrenoceptors in the central nervous system. Acta Vet Scand Suppl. 1989; 85:11–19. [PubMed: 2571258]

Sedlacik J, Boelmans K, Lobel U, Holst B, Siemonsen S, Fiehler J. Reversible, irreversible and effective transverse relaxation rates in normal aging brain at 3T. Neuroimage. 2014; 84:1032–1041. [PubMed: 24004692]

Sicard KM, Duong TQ. Effects of hypoxia, hyperoxia, and hypercapnia on baseline and stimulus-evoked BOLD, CBF, and CMRO2 in spontaneously breathing animals. Neuroimage. 2005; 25:850–858. [PubMed: 15808985]

Silvennoinen MJ, Clingman CS, Golay X, Kauppinen RA, van Zijl PC. Comparison of the dependence of blood R2 and R2* on oxygen saturation at 1.5 and 4.7 Tesla. Magn Reson Med. 2003; 49:47–60. [PubMed: 12509819]

Smith AJ, Blumenfeld H, Behar KL, Rothman DL, Shulman RG, Hyder F. Cerebral energetics and spiking frequency: the neurophysiological basis of fMRI. Proc Natl Acad Sci U S A. 2002; 99:10765–10770. [PubMed: 12134056]

Stables LA, Kennan RP, Gore JC. Asymmetric spin-echo imaging of magnetically inhomogeneous systems: theory, experiment, and numerical studies. Magn Reson Med. 1998; 40:432–442. [PubMed: 9727947]

Stefanovic B, Warnking JM, Rylander KM, Pike GB. The effect of global cerebral vasodilation on focal activation hemodynamics. Neuroimage. 2006; 30:726–734. [PubMed: 16337135]

Thesen T, Leontiev O, Song T, Dehghani N, Hagler DJ Jr, Huang M, Buxton R, Halgren E. Depression of cortical activity in humans by mild hypercapnia. Hum Brain Mapp. 2012; 33:715–726. [PubMed: 21500313]

Ueki M, Mies G, Hossmann KA. Effect of alpha-chloralose, halothane, pentobarbital and nitrous oxide anesthesia on metabolic coupling in somatosensory cortex of rat. Acta Anaesthesiol Scand. 1992; 36:318–322. [PubMed: 1595336]

Weber R, Ramos-Cabrer P, Wiedermann D, van Camp N, Hoehn M. A fully noninvasive and robust experimental protocol for longitudinal fMRI studies in the rat. Neuroimage. 2006; 29:1303–1310. [PubMed: 16223588]

Winters WD. Effects of drugs on the electrical activity of the brain: anesthetics. Annu Rev Pharmacol Toxicol. 1976; 16:413–426. [PubMed: 779620]

Xu F, Uh J, Brier MR, Hart J Jr, Yezhuvath US, Gu H, Yang Y, Lu H. The influence of carbon dioxide on brain activity and metabolism in conscious humans. J Cereb Blood Flow Metab. 2011; 31:58–67. [PubMed: 20842164]

Yablonskiy DA, Haacke EM. An MRI method for measuring T2 in the presence of static and RF magnetic field inhomogeneities. Magn Reson Med. 1997; 37:872–876. [PubMed: 9178238]

Zappe AC, Uludag K, Oeltermann A, Ugurbil K, Logothetis NK. The influence of moderate hypercapnia on neural activity in the anesthetized nonhuman primate. Cereb Cortex. 2008; 18:2666–2673. [PubMed: 18326521]

Zhao F, Zhao T, Zhou L, Wu Q, Hu X. BOLD study of stimulation-induced neural activity and resting-state connectivity in medetomidine-sedated rat. Neuroimage. 2008; 39:248–260. [PubMed: 17904868]

Highlights

- For calibrated fMRI the parameter M across brain regions is determined from the dynamic range of the BOLD signal.
- M was mapped by R_2', given by difference between relaxation rates of gradient- and spin-echo.
- M-values measured across two brain states in rats were found to be homogeneous in the neocortex.
- While M-values in cortex were state-dependent, M-values in white matter and diencephalon were indifferent across states.

ARTWORKS WITH CAPTIONS

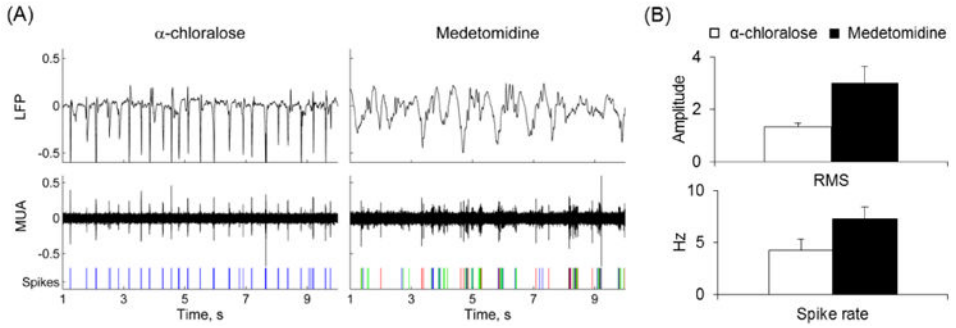

Figure 1.

Neural activities for rats anesthetized with α-chloralose vs. medetomidine. **(A)** LFP and MUA recorded from the $S1_{FL}$ area in rats. Spikes of different classes from MUA are shown on the bottom panel. LFP and MUA under α-chloralose showed a regular though sparser activation pattern compared to medetomidine anesthesia. **(B)** Root mean square of LFP amplitude (mean±SD) and the spike rate (mean±SD) from MUA recordings for rats with α-chloralose (n=3) and medetomidine (n=3). The α-chloralose group had an LFP_{RMS} of 1.3±0.1 and a spike rate of 4.2±1.1Hz. On the other hand, the medetomidine group had an LFP_{RMS} of 3.0±0.7 and a spike rate of 7.3±1.1Hz. Compared to the α-chloralose group, the neural activity in the medetomidine group was ∼100% higher ($p < 0.05$).

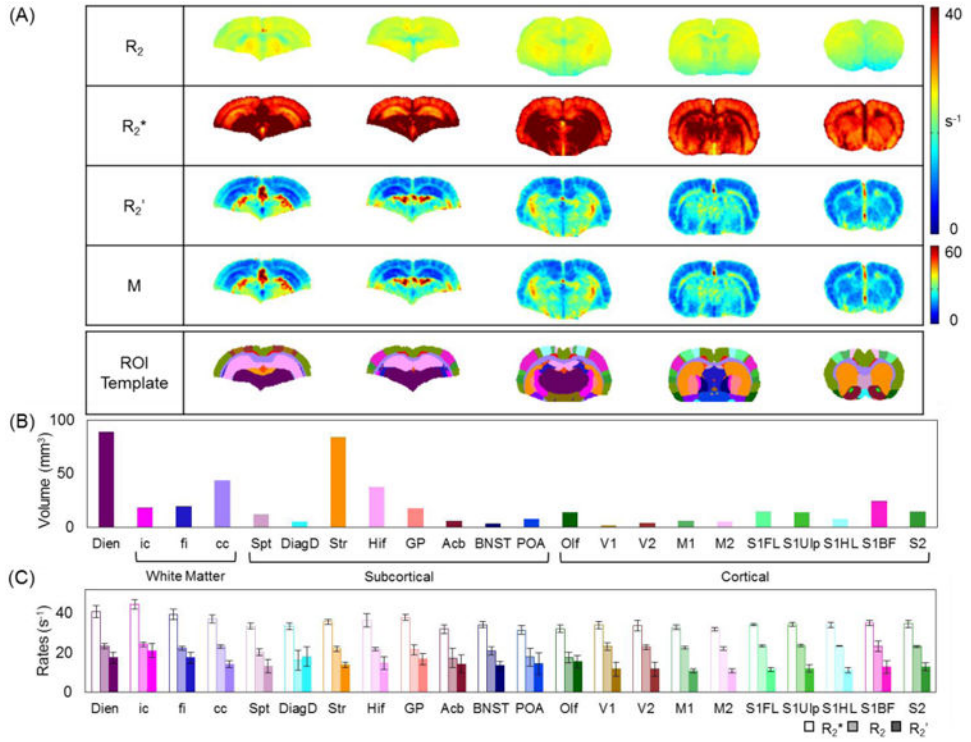

Figure 2.

Summary of transverse relaxation rates (R_2, R_2*, R_2') and M measured with α-chloralose. **(A)** Mean R_2, R_2*, R_2', and M maps (n=8) for representative slices, where the bottom column shows the brain template of 22 ROIs onto which all maps were registered. **(B)** Volume of each ROI covered by the brain template, which includes 8 ROIs in the subcortex, 10 ROIs in the cerebral cortex, 3 ROIs in white matter, and the diencephalon. The abbreviations of these ROIs are in Materials and Methods. The subcortical and cortical regions accounted for 39% and 23%, respectively, of the total volume, whereas white matter and diencephalon covered 18% and 20%, respectively. **(C)** Mean R_2, R_2*, and R_2' in each ROI, where the error bars indicate SD. Among all ROIs, R_2 ranged from 16.1 s^{-1} to 24.1 s^{-1}, R_2* ranged from 31.4 s^{-1} to 44.5 s^{-1}, and R_2' ranged from 10.6 s^{-1} to 20.9 s^{-1}. In general, the regional variations were smaller in cortex, where R_2 was 22.4±2.2 s^{-1}, R_2* was 33.9±3.1 s^{-1}, and R_2' was 11.5±3.3 s^{-1}; but in subcortex they were 21.2±2.4 s^{-1}, 35.7±6.1 s^{-1}, and 14.2±5.8 s^{-1}. Among the cortical ROIs, R_2' was smallest in the motor region (M1, 10.6±1.1 s^{-1}) and largest in olfactory structure (Olf, 15.4±3.2 s^{-1}). Among the subcortical regions R_2' was smallest in septum (Spt, 13.1±3.5 s^{-1}) and largest in diagonal domain (DiagD, 17.9±4.9 s^{-1}).

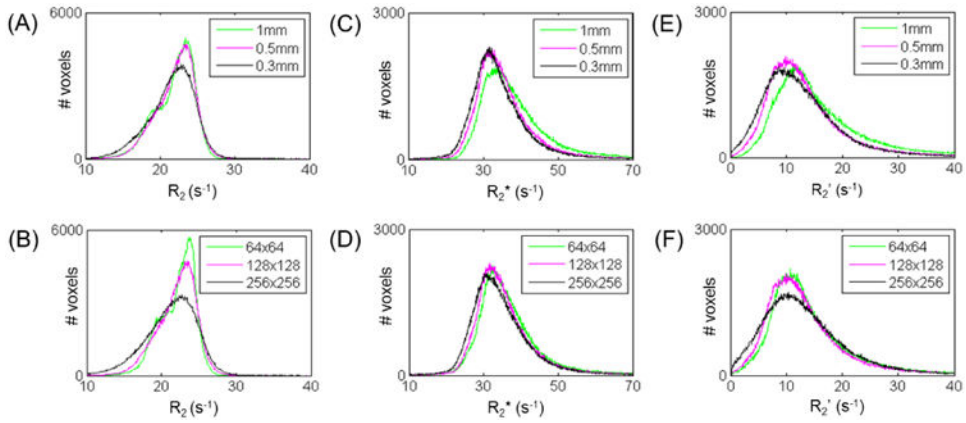

Figure 3.

Dependencies of relaxation rate (R_2, R_2*, R_2') measurements at different imaging resolutions for through-plane (i.e., by varying slice thickness, top panels) and in-plane (i.e., by varying image matrix, bottom panels). Data shown for the same subject with α-chloralose, where histograms represent all 22 ROIs in the brain template of Figure 2B. **(A, B)** Compared to R_2 at default setting, R_2 remained similar with matrix size or slice thickness. **(C, D)** Compared to R_2* at default settings, R_2* remained similar at different image matrix or slice thickness. **(E, F)** Compared to R_2' at default setting, R_2' did not change significantly ($p > 0.05$) at different image matrix size or with thinner slices. See Supplementary Figure 3 for SNR of images with different imaging resolutions. See also Table 2.

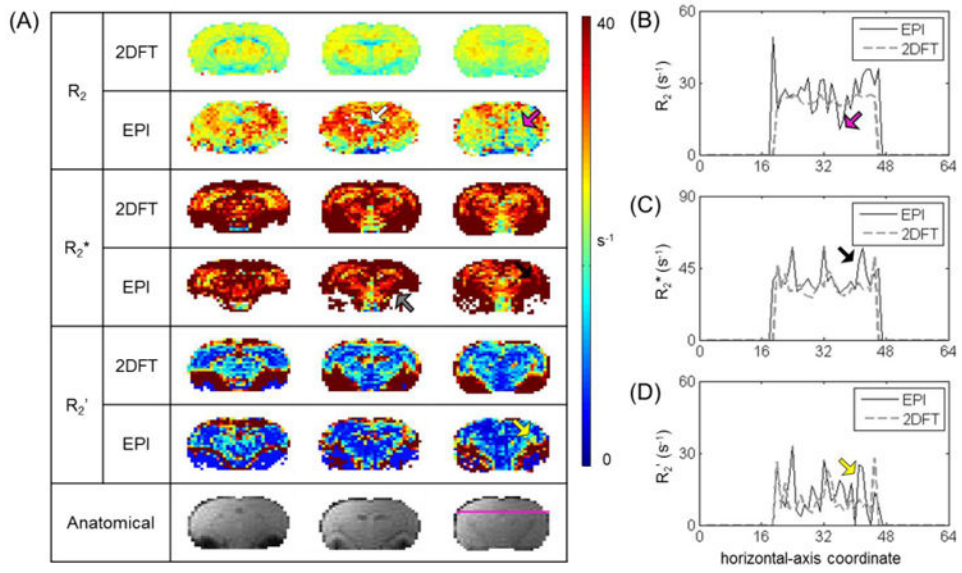

Figure 4.

Comparison of R_2, R_2*, R_2' measured by different sequences. Maps and data shown are for the same subject as Figure 3, with the same through-plane and in-plane resolutions. (A) Raw images of R_2, R_2*, R_2', and M measured by 2DFT (top) vs. EPI (bottom). The lowest panel shows corresponding anatomical images. Comparison shows some distinctive features of the EPI for specifically difficult to shim regions (indicated by colored arrows). R_2 in EPI was more heterogeneous than in 2DFT (magenta arrow); EPI gave higher overall R_2, except in hippocampal formation (brown arrow). For R_2* in EPI, strong magnetic susceptibility not only affected R_2* fitting through signal drop out (gray arrow), but also resulted in heterogeneity in nearby regions (red arrow); due to the heterogeneities in R_2 and R_2* with EPI, R_2' with EPI was less uniform (yellow). M followed the same trend as R_2'. (B-D) R_2, R_2*, and R_2' values horizontally across the coronal slice, as traced out by a purple line on the anatomical image in (A). Colored arrows point to some features discussed in (A). Compared to 2DFT, generally EPI gave higher R_2 values with greater variation in R_2*, thus leading to a larger extent of regional heterogeneity in R_2' and M.

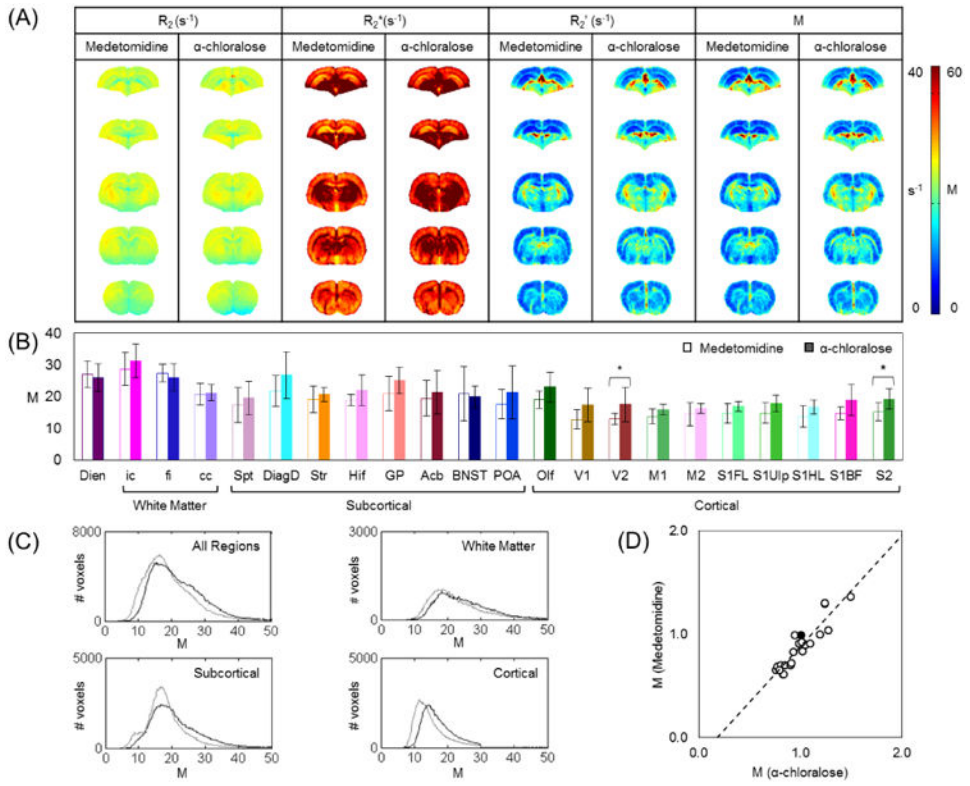

Figure 5.

Comparison of M across different brain states. **(A)** Mean R_2, R_2*, and M maps for representative slices in α-chloralose (n=8) and medetomidine (n=7) anesthetized rats. **(B)** M for each ROI (mean±SD) with α-chloralose (filled bars) vs. medetomidine (open bars). Regions of maximum and minimum M were very similar among α-chloralose and medetomidine. M_{med} in cortex was lowest in V1 (12.8±3.0) and highest in olfactory structure (19.1±2.7), while subcortically M_{med} was smallest in Septum (17.4±5.5) and largest in diagonal domain (21.8±4.8). Student's t-test between M_α and M_{med} gave significance two small cortical regions (V2, S2; $p < 0.05$). Two-way ANOVA test indicated that M_{med} were significantly lower than M_α in both cortical ($p < 0.001$) and subcortical regions ($p < 0.05$), but not in white matter ($p > 0.05$) and diencephalon ($p > 0.05$). **(C)** Distribution of M in all regions, for white matter, subcortical, and cortical regions. Measurements made in the α-chloralose group are traced in black lines, and those in the medetomidine group are traced in gray lines. Among all the regions, M_α was 22.2±8.5 and M_{med} was 19.6.±8.2. In the subcortical regions, M_α was 21.7±9.0 and M_{med} was 18.7±7.9. In the cortical regions, M_α was 17.3±4.8 and M_{med} was 14.7±4.7. In white matter, M_α was 23.6±7.8 and M_{med} was 22.5±8.0. **(D)** With M in cc (center black circle) as the normalization factor, magnitudes of normalized M_{med} in all ROIs were highly correlated to normalized M_{med} ($r^2 = 0.85$), which corresponded to the trend observed in (B).

Table 1

Physiological information from blood pressure and blood gases.

Physiological Parameters	Measured Value
Blood pressure (mmHg)	90±10
pH	7.4±0.2
pO_2 (mmHg)	37±3
pO_2 (mmHg)	100±15

Table 2

Relaxation rate (R_2, R_2*, R_2') measurements at varying slice thickness and in-plane image matrices. All data with same FOV. See also Figure 3.

Resolution (in-plane matrix, slice thickness)	R_2 (s^{-1})	R_2* (s^{-1})	R_2' (s^{-1})
128×128, 0.5 mm	22.0±2.7	35.9±9.6	14.1±9.5
256×256, 0.5 mm	21.1±3.7	34.8±9.1	13.9±9.2
64×64, 0.5 mm	22.1±2.3	37.4±10.8	15.4±11.0
128×128, 0.3 mm	21.5±3.1	34.7±9.6	13.4±9.5
128×128, 1 mm	21.9±2.6	39.2±12.6	17.4±12.8